THE JOURNAL OF PHYSICAL CHEMISTRY B

ARTICLE

pubs.acs.org/JPCB

Alteration of the H-Bond to the A_{1A} Phylloquinone in Photosystem I: Influence on the Kinetics and Energetics of Electron Transfer

Nithya Srinivasan,[†] Stefano Santabarbara,[‡,+] Fabrice Rappaport,[‡] Donatella Carbonera,[§] Kevin Redding,[⊥] Art van der Est,[∥,*] and John H. Golbeck[*,†,¶]

[†]Department of Biochemistry and Molecular Biology. [¶]Department of Chemistry, The Pennsylvania State University, University Park, Pennsylvania 16802, United States

[‡]Institut de Biologie Physico-Chimique, UMR 7141 CNRS/UPMC, 13 Rue Pierre et Marie Curie, 75005 Paris, France

[§]Department of Chemical Sciences, University of Padua, Via Marzolo 1, 35131 Padova, Italy

[⊥]Department of Chemistry and Biochemistry, Arizona State University, Tempe, Arizona 85287, United States

[∥]Department of Chemistry, Brock University, 500 Glenridge Avenue, St. Catharines, Ontario L2S 3A1, Canada

Supporting Information

ABSTRACT: In Photosystem I, the backbone nitrogen of $Leu722_{PsaA}$ forms a hydrogen bond with the C_4 carbonyl oxygen of phylloquinone in the A_{1A} site. A previous low-temperature EPR study indicated that substitution of $Leu722_{PsaA}$ with a bulky Trp residue results in a weakened H-bond. Here, we employ room temperature, time-resolved optical spectroscopy and variable temperature, transient EPR spectroscopy to probe the effect of the altered H-bond on the energetics and kinetics of electron transfer. Relative to the wild type, we find that the rate of electron transfer from A_{1A}^- to F_X in the $L722W_{PsaA}$ variant is faster by a factor of 3. This change is attributed to a lowered midpoint potential of A_{1A}/A_{1A}^-, resulting in a larger Gibbs free energy change between A_{1A}/A_{1A}^- and F_X/F_X^-. An activation energy of 180 ± 10 meV is determined for the A_{1A}^--to-F_X forward electron transfer step in the $L722W_{PsaA}$ variant compared with 220 ± 10 meV in the wild type. The Arrhenius plot shows a break at ∼200 K, below which the rate becomes nearly independent of temperature. This behavior is described using a quantum mechanical treatment that takes the zero-point energy into account as well as an alternative model that invokes a dynamical transition in the protein at ∼200 K.

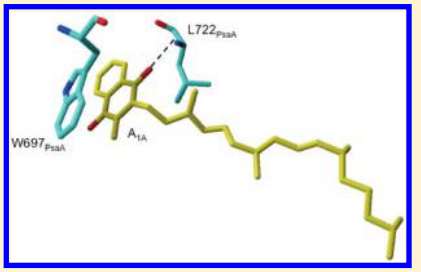

INTRODUCTION

All naturally occurring reaction centers share a common structural motif that consists of a membrane-bound protein dimer and a contingent of electron transfer cofactors that carry out light-induced charge separation.[1] In Photosystem I (PS I), the majority of the cofactors are bound by the PsaA/PsaB heterodimer and are arranged symmetrically about a pseudo-C_2 axis of symmetry. Although the details of the initial steps of charge separation are still under investigation,[2] there is now a consensus that electron transfer occurs via two branches of cofactors on the PsaA and PsaB polypeptides. These consist of a pair of chlorophyll *a*′/chlorophyll *a* molecules (P_{700}), two intermediate chlorophyll *a* molecules (A_A and A_B), two acceptor chlorophyll *a* molecules (A_{0A}/A_{0B}), two phylloquinones (A_{1A}/A_{1B}), and an interpolypeptide [4Fe−4S] cluster, F_X.[3−9] The terminal [4Fe−4S] clusters F_A and F_B, which are located on the membrane-extrinsic PsaC subunit, serve to vector the electrons out of the membrane phase to soluble ferredoxin or flavodoxin.

The phylloquinones in the A_{1A} and A_{1B} sites of PS I possess some of the most negative midpoint potentials in biology.[10] Early estimates placed their midpoint potentials in the vicinity of −700 to −800 mV,[11,12] and recent theoretical and modeling studies have indicated values of −531,[9] −671,[13] and −678 mV[14] for A_{1A}, and values of−688,[9] −700,[14] and −844 mV[13] for A_{1B}. The midpoint potential of F_X falls in a more narrow range, with a value centered about −655 ± 35 mV based on both experimental and theoretical studies (see ref 7 for a detailed discussion of the redox potentials of the PS I cofactors). Thus, there is widespread agreement that the A_{1B}-to-F_X electron transfer step is thermodynamically favorable, but there is more uncertainty about the A_{1A}-to-F_X electron transfer step, which is isoenergetic or, at best, mildly unfavorable. Accordingly, the activation energy for electron transfer from A_{1A} to F_X should be larger than that from A_{1B} to F_X. In keeping with these findings, a thermally activated slow phase[15] and a weakly activated fast phase[16] are observed experimentally and are attributed to electron transfer from A_{1A}^- and A_{1B}^- to F_X, respectively.

The origin of the highly negative midpoint potentials of the phylloquinones is not completely understood; however, it is clear that protein−quinone interactions must play a significant role. One such interaction especially merits attention. $Leu722_{PsaA}$

Received: October 4, 2010
Revised: December 20, 2010
Published: February 7, 2011

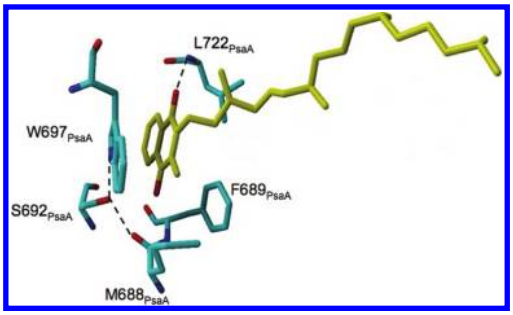

Figure 1. The A-branch phylloquinone binding pocket of PS I. The H-bond formed between Leu722$_{PsaA}$ and the C_4 carbonyl oxygen atom of the A_{1A} phylloquinone is depicted along with the π-stacked Trp residue W697$_{PsaA}$.

(Leu706$_{PsaB}$) provides a single H-bond via a backbone N to the C_4 carbonyl oxygen of the A_{1A} (A_{1B}) phylloquinone (Figure 1). In a recent study, the H-bonded Leu722$_{PsaA}$ was replaced with a bulky Trp residue.[17] The partially resolved hyperfine couplings in the low temperature spin-polarized transient EPR spectrum of the P_{700}^+ A_{1A}^- radical pair were diminished due to an altered spin density distribution on the A_{1A}^- phyllosemiquinone, consistent with a weaker H-bond. One consequence of this alteration should be a lower midpoint potential for the A_{1A}^- phylloquinone and, hence, a faster rate of electron transfer from A_{1A}^- to F_X. In a study performed at 240 K, this was found to be the case.[18] This finding was supported by a study in *Chlamydomonas reinhardtii* in which the substitution of the H-bonded Leu residues on the A- and B-branches by a Tyr or Thr residue resulted in the acceleration of the slow and fast kinetic phases of A_1^- oxidation, respectively.[19]

In this paper, we expand the study of the L722W$_{PsaA}$ variant to include kinetic data from room temperature, time-resolved optical spectroscopy and variable temperature, transient EPR spectroscopy. Our results show an increase in the rate of forward electron transfer from A_{1A}^- to F_X consistent with the expected lower midpoint potential of A_{1A}/A_{1A}^- as a consequence of a weakened H-bond. Temperature dependence studies show that there are two distinct temperature regimes above and below ~200 K. Above this temperature, the behavior is similar to the wild type but with a lower activation energy. Below ~200 K, the A_{1A}^--to-F_X electron transfer in the L722W$_{PsaA}$ variant becomes nearly activationless and, hence, more like the A_{1B}^--to-F_X step in the wild type.[16] We propose that this difference is a result of either a change in the frequency of the vibrational mode coupled to the electron transfer or a change in the influence of the slow protein motions associated with a dynamic transition at ~200 K.

MATERIALS AND METHODS

Cell Culture and PS I Isolation. *Synechocystis* sp. PCC 6803 wild type and variant strains were cultured in β-HEPES medium with 5 mM glucose under low light intensity. The preparation of thylakoid membranes and the isolation of PS I trimers were carried out as described in ref 20.

Steady State Electron Transfer Rates of Flavodoxin Photoreduction. Steady state electron transfer rates of flavodoxin photoreduction were measured using wild type and variant PS I complexes at 5 μg of Chl/mL in 50 mM Tris/HCl, pH 8.3. A typical sample contained 50 mM $MgCl_2$, 6 μM phenazine methosulfate, 20 μM cytochrome c_6, 15 μM flavodoxin, 6 mM sodium ascorbate, and 0.05% *n*-dodecyl-β-D-maltopyranoside. Measurements were made by monitoring the rate of change in the absorption at 580 nm using a Cary 50 Bio UV−visible spectrophotometer with blocking filters for the actinic and measuring beams. The actinic illumination was provided by high-intensity red light-emitting diodes (Hansatech Instruments).

Out-of-Phase Echo Modulation. Electron spin−echo (ESE) amplitude-modulation curves were obtained on a Bruker EleXsys E580 spectrometer by collecting the amplitude of the echo in the out-of-phase channel. The echo height was measured at time $T \approx \tau_2$ after the second microwave pulse of a laser flash−τ_1−90−τ_2−180 pulse sequence as a function of τ_2 (see ref 21 for details).

Time-Resolved Optical Spectroscopy at 480 nm. The kinetics of A_{1A}^- and A_{1B}^- oxidation were measured optically in the nanosecond time scale using a time-resolved spectrophotometer similar to that described in ref 22, except in this study, the flash-induced transient absorption changes were monitored at 480 nm. The 480 nm measuring beam was filtered using a combination of narrow-band (8 nm) interference and colored glass filters (to block the scattered laser flash). All spectroscopic measurements were performed at room temperature. Kinetic traces were analyzed by fitting with a multiexponential function using the Marquardt least-squares algorithm that was programmed in IGOR Pro v. 5.2 (Wavemetrics, Lake Oswego, OR).

Pump−Probe Optical Spectroscopy in the Near-UV and Visible Region. Measurements of the kinetics of semiquinone oxidation in the nanosecond to microsecond time scale were performed on isolated PS I trimers in a pump−probe spectrophotometer as described previously.[23] The PS I complexes were suspended at a concentration of 40 μg/mL in 50 mM Tris buffer with sodium ascorbate and DCPIP concentrations of 10 mM and 40 μM, respectively. Decay-associated spectra of the kinetic phases were derived from a global, multiexponential fit of the kinetic components obtained at each wavelength using the program MEXFIT adapted from ref 24. Charge separation was induced by a 5- ns (full width at half-maximum) light pulse at 700 nm using a Nd:YAG pumped LDS 698 dye exciting ~70% of the PS I complexes. Absorbance changes were followed from 5 ns to 20 μs using detecting flashes provided by an OPO Continuum (OPO Panther, type II) from 300 to 540 nm, frequency-doubled for wavelengths less than 410 nm. For detection in the UV, a fluorescent glass (Sumita Optical Glass, Lumilass-B) was used to convert the UV photons to blue photons to minimize noise.

Optically Detected Magnetic Resonance. The setup used to record fluorescence detected magnetic resonance (FDMR) has been previously described in ref 25. All samples were diluted to a concentration equivalent to 100 μg Chl/mL in a buffer containing 0.1 M sorbitol, 10 mM NaCl, 5 mM $MgCl_2$, and 60% w/v glycerol immediately before measurement. Prior reduction of PS I electron acceptors was accomplished by a photoaccumulation procedure as described by Carbonera et al.[25] with minor modifications. Sodium dithionite was added to the sample to a final concentration of 10 mM, incubated under anaerobic conditions in the dark for 5 min, diluted into glycerol-containing buffer to a final concentration of 60% w/v, and illuminated for 5 min with focused white light from a 600-W halogen lamp. Deconvolution of the FDMR spectra in terms of Gaussian bands was carried out as described elsewhere.[25−27]

Transient EPR Spectroscopy. X-band (9 GHz) transient EPR experiments were carried out on a laboratory-built spectrometer using a modified Bruker 200D-SRC spectrometer

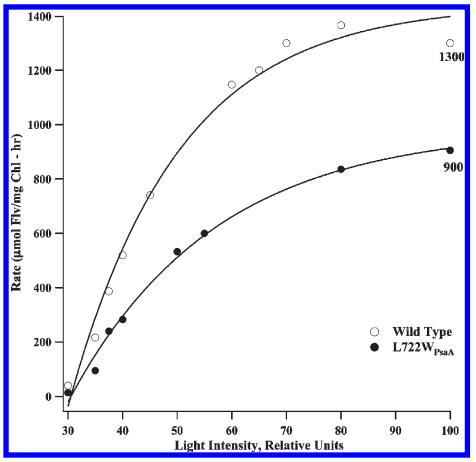

Figure 2. Steady-state rates of flavodoxin photoreduction in PS I complexes isolated from wild type (○) and L722W$_{PsaA}$ (●) in μmol flavodoxin mg Chl^{-1} hr^{-1} plotted against relative light intensity.

equipped with an ER-4118XMD-5W1 dielectric ring resonator and an Oxford CF935 helium gas flow cryostat. The loaded Q value for this dielectric ring resonator was about Q= 3000, equivalent to a rise time of $\tau_r = Q/(2\pi \times \nu_{mw}) \approx 50$ ns. All samples contained 1 mM sodium ascorbate and 50 μM phenazine methosulfate as the external electron donor in 50 mM Tris buffer at pH 8.3 and were frozen in the dark. The samples were illuminated at 532 nm using the second harmonic of a Continuum Surelite Nd YAG laser operating at 10 Hz.

RESULTS

Prior to presenting variable temperature studies of the kinetics of the A_{1A}^--to-F_X electron transfer step, we briefly describe the overall electron transfer throughput and the position and orientation of the A_{1A} phylloquinone in PS I complexes from the L722W$_{PsaA}$ variant.

Electron Transfer Throughput. Any block in electron transfer through the A_{1A} phylloquinone should be reflected in a corresponding change in the rate of flavodoxin reduction under steady-state illumination. The rates of flavodoxin reduction supported by the wild type and L722W$_{PsaA}$ variant under near-saturating light conditions were 1300 μmol mg Chl^{-1} hr^{-1} and 900 μmol/mg Chl^{-1} hr^{-1}, respectively. The light dependencies of flavodoxin reduction in the L722W$_{PsaA}$ variant and the wild type, however, are comparable (Figure 2). This indicates that the optical cross section of PS I is unaltered in the L722W$_{PsaA}$ variant. Assuming 100 Chl/P_{700}, these rates correspond to 36 e$^-$ PS I^{-1} s^{-1} for the wild type and 25 e$^-$ PS I^{-1} s^{-1}for the L722W$_{PsaA}$ variant.

The lower rate of electron throughput in the L722W$_{PsaA}$ variant suggests that A_{1A} may be missing or inactive in a fraction of the PS I complexes. If so, charge separation in the A branch would lead to formation of $^3P_{700}$ during charge recombination from $P_{700}^+A_0^-$, which typically occurs with a lifetime of ~30 ns.[28,29] Support for the occurrence of charge recombination can be drawn from an analysis of the yield of $^3P_{700}$ as measured by fluorescence-detected magnetic resonance (FDMR). FDMR spectra of thylakoid membranes isolated from the wild type and the L722W$_{PsaA}$ variant are shown in Figure S1 in the Supporting Information. Assignment of the FDMR signal to $^3P_{700}$ was confirmed both by determination of the zero-field splitting parameters and by recording the microwave-induced

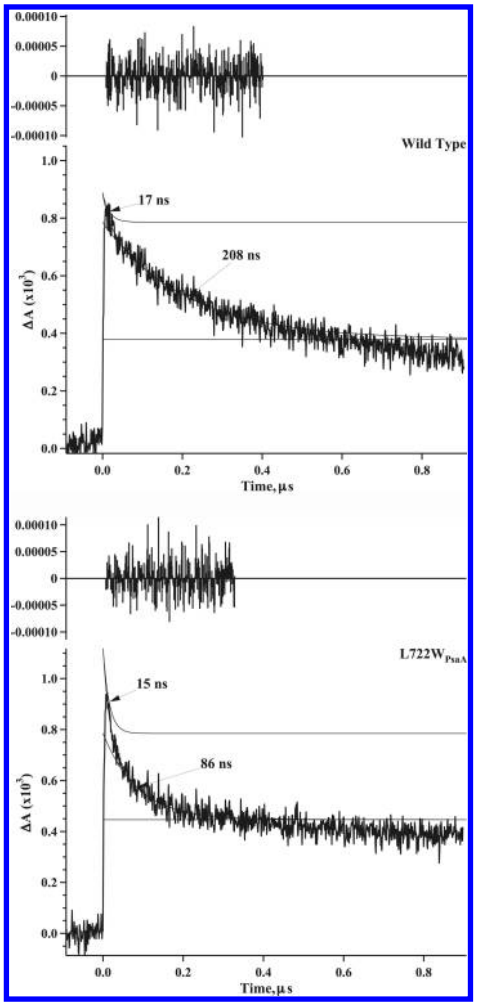

Figure 3. Time-resolved optical kinetics at 480 nm from wild type (top) and L722W$_{PsaA}$ (bottom). The data is presented with a linear time axis so that the lifetime and contributions of the two phases can be readily distinguished. The residuals for each fit are shown above the main trace.

triplet minus singlet spectrum, which is virtually identical in the wild type and the L722W$_{PsaA}$ variant. FDMR measurements on illuminated samples with the terminal acceptors reduced and oxidized indicate that 9−12% of the PS I complexes from the L722W$_{PsaA}$ variant generate triplets, compared with the 2−4% of PS I complexes from the wild type. In contrast, we did not find evidence for $^3P_{700}$ by transient EPR in the initial study of this mutant.[17]

Position and Orientation of A_{1A}. In principle, the weakened H-bond in the L722W$_{PsaA}$ variant could be accompanied by a change in the position or orientation of the A_{1A} phylloquinone. However, analysis of the low-temperature, spin-polarized EPR spectra of $P_{700}^+A_{1A}^-$ reported previously[17] provides no evidence for a change in the orientation of A_{1A}. Out-of-phase electron spin echo envelope modulation (OOP-ESEEM) experiments allow the distance between the center of the electron spin distribution of the P_{700}^+ and A_{1A}^- radicals to be measured (see ref 30 for a review) and provide a sensitive indicator of changes in the position of A_{1A}. Analysis of the OOP-ESEEM signal of the radical pair $P_{700}^+A_{1A}^-$ in the wild type and the L722W$_{PsaA}$ variant (Figure S2 in the Supporting Information) indicates that the position of A_{1A} relative to P_{700} is also unaltered. Disorder in the binding site would be expected to cause a distribution of

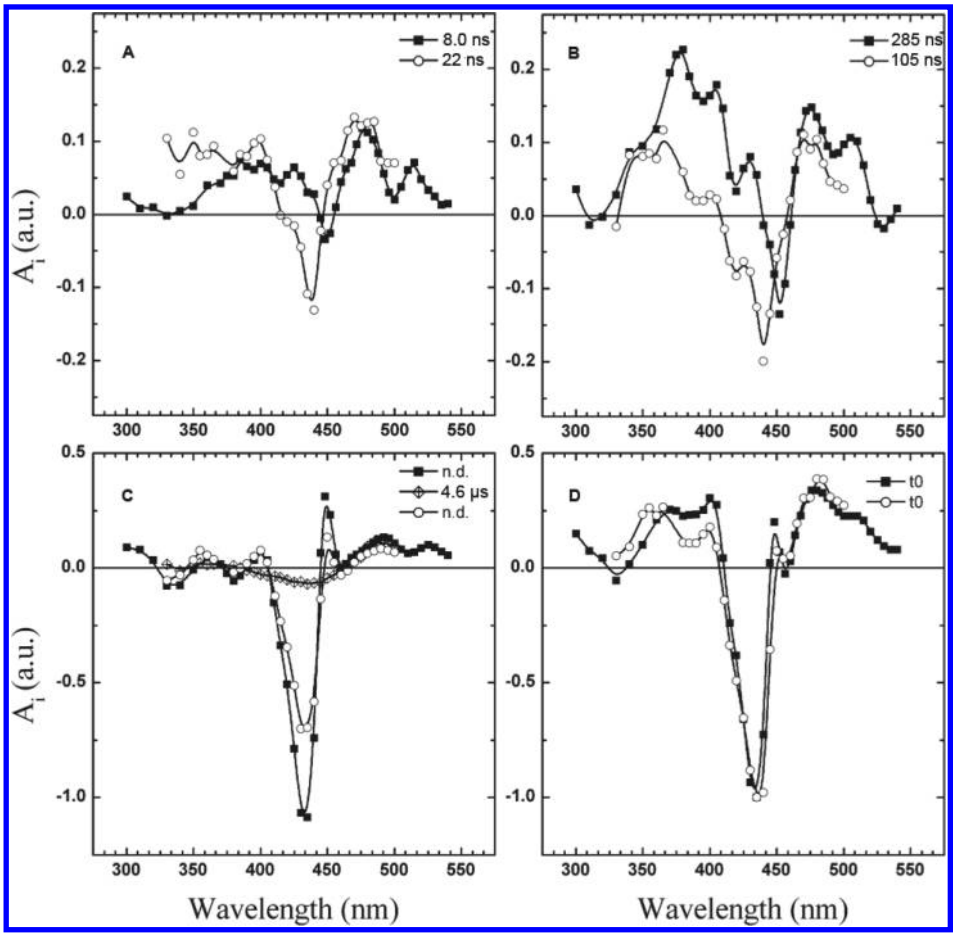

Figure 4. Spectra of the kinetic phases obtained by global decomposition of the pump−probe optical spectroscopy experiment on PS I complexes isolated from wild type (closed symbols) and L722W$_{PsaA}$ variant (open symbols) in the near-UV and blue region. Panel A: comparison of the fast kinetic component. Panel B: comparison of the slow kinetic component. Panel C: nondecaying component together with the kinetic component representing the recombination event in L722W$_{PsaA}$. Panel D: normalized initial spectra extrapolated to time zero (t_0).

distances and modulation frequencies, which would lead to the damping of the modulation curve.[21,30] Because no difference in the decay of the modulation was observed for the L722W$_{PsaA}$ variant and the wild type, the phylloquinone in the A$_{1A}$ site does not experience greater disorder as a result of the presence of the substitution.

Time-Resolved Optical Measurements. Figure 3 depicts flash-induced absorption changes in the nanosecond-to-microsecond time scale in PS I trimers isolated from the wild type and the L722W$_{PsaA}$ variant. The measurement was carried out at 480 nm, a wavelength at which the phyllosemiquinone anion induces an electrochromic bandshift in a nearby carotenoid.[5] The kinetic traces obtained at 480 nm are similar to those at 380 nm, except that a positive contribution due to long-lived P_{700}^+ is also observed. In addition, the measurement should be independent of any spectral shifts in the near-UV induced by an alteration of the H-bond. Biexponential fits for PS I from the wild type yield lifetimes of 17 and 208 ns for the two kinetic phases, with extrapolated relative amplitudes of 0.21 and 0.79, respectively. Similar fits for PS I from the L722W$_{PsaA}$ variant yield lifetimes of 15 and 86 ns for the two kinetic phases, with extrapolated relative amplitudes of 0.47 and 0.53, respectively. The major effect is therefore a change in the lifetime of the slow kinetic phase, whereas the fast kinetic phase remains unchanged. This is in agreement with the currently accepted paradigm in which the fast kinetic phase represents B-branch electron transfer from A_{1B}^- to F_X, and the slow kinetic phase represents A-branch electron transfer from A_{1A}^- to F_X.

To obtain further insight from the alterations of lifetimes and amplitudes of the kinetic phases that describe A_1^- oxidation, transient absorption changes were measured at several wavelengths in the near-UV and blue region by pump−probe optical spectroscopy and analyzed by a global fitting routine. Three kinetic components were obtained: two that decay in the nanosecond time range, which are associated with the fast and slow oxidation of A_1^-, and one that is long-lived, which does not decay within the detection time of the experiment and is associated with P_{700}^+ reduction. An additional 4 μs phase with a small amplitude is observed in the L722W$_{PsaA}$ variant only. In accordance with previously published data,[22] this component is not resolved in wild type PS I trimers.

The decay-associated spectra (DAS) of all components normalized to the initial absorbance change at time zero for both wild type and the L722W$_{PsaA}$ variant are depicted in Figure 4. Panel A shows the fast phase due to A_{1B}^--to-F_X electron transfer; panel B shows the slow phase due to A_{1A}^--to-F_X electron transfer; panel C shows the nondecaying phase together with the additional 4 μs phase obtained for L722W$_{PsaA}$, and panel D shows the normalized initial spectra extrapolated to time zero. The spectrum of the nondecaying component is similar to that of

the P_{700}^{+} $[F_A/F_B]^{-}$ minus P_{700} $[F_A/F_B]$ difference spectrum.[31] The two nanosecond time components display positive absorption bands between 370 and 400 nm and are characteristic of the oxidation of A_{1A}^{-} and A_{1B}^{-}.

These spectra also show positive changes between 370 and 400 nm and a bathochromic band shift of a carotenoid centered around 450 nm. A change in the lifetime of the decay as well as striking changes in the shape of the DAS are observed in the $L722W_{PsaA}$ variant. The major effect is a change in the lifetime of the slow kinetic phase, which decreases from 285 ± 12 ns in the wild type to 105 ± 9 ns in the $L722W_{PsaA}$ variant. The fast kinetic phase remains relatively unchanged. In agreement with the single wavelength study at 480 nm, the ratio of the fast to the slow component is higher in the $L722W_{PsaA}$ variant (relative amplitudes at 370 nm of 0.50 to 0.50) than in the wild type sample (relative amplitudes at 380 nm of 0.20 and 0.80).

A similar redistribution of the kinetic phases of A_1^{-} oxidation as well as an acceleration in the kinetics has been observed in variants of *C. reinhardtii* that target the H-bond.[19] It was proposed that the redistribution results from the suppression of a transient interquinone electron transfer, mediated by F_X, which is promoted in the wild type by the difference in midpoint redox potentials between the two phylloquinones. Because A_{1A}^{-} is estimated to be more oxidizing than A_{1B}^{-}, the electron can transfer from one quinone to the other. Any process that reduces the driving force for this reaction (for instance, a more reducing potential for A_{1A}^{-}) would have the effect of diminishing the transfer and, hence, increasing the relative amplitude of the fast phase with respect to the slow phase,[19] which is what is observed here.

Apart from the change in relative amplitudes of the fast and slow phases of A_1^{-} oxidation, the DAS also shows a hypsochromic shift in the blue region, with the otherwise dominant peak at 380 nm occurring at ~370 nm in the $L722W_{PsaA}$ variant. A marked trough is observed in the 435−445 nm region in the DAS of the nanosecond components. Similar alterations in the DAS of nanosecond kinetic phases were previously observed in mutants of the A_0 binding site[32] and attributed to the occurrence of charge recombination reactions between P_{700}^{+} and A_0^{-}, which are known to take place with a lifetime of ~30 ns[28,29] and to exhibit similar transient absorption difference spectra. Charge recombination would also generate $^3P_{700}$, which decays in 4 μs and accounts for the additional kinetic component observed in PS I from the $L722W_{PsaA}$ variant. A similar conclusion was drawn from experiments on whole cells (Figure S3 in the Supporting Information) indicating that these differences are not artifacts due to perturbation of A_{1A} binding in $L722W_{PsaA}$ induced during the isolation of PS I.

Room Temperature, Spin-Polarized, Transient EPR Measurements of Forward Electron Transfer. For wild type PS I, two consecutive polarization patterns are observed in the transient EPR data at temperatures above 220 K.[33] As the electron is transferred from A_{1A}^{-} to F_X, the E/A/E polarization pattern (early spectrum) due to the $P_{700}^{+}A_{1A}^{-}$ radical pair changes to one with net emission (late spectrum) that arises from the P_{700}^{+} contribution to the $P_{700}^{+}(Fe/S)^{-}$ radical pair. Although it is known that electron transfer proceeds via F_X,[34] the radical pair is referred to as $P_{700}^{+}(Fe/S)^{-}$ to allow for the possibility that the F_X^{-}-to-F_A step is faster than the A_{1A}^{-}-to-F_X step.[32] Only the slow phase of electron transfer from A_{1A}^{-} to F_X that occurs via the A-branch is kinetically resolved by transient EPR. The kinetic phase due to A_{1B}^{-}-to-F_X electron transfer through the B branch occurs faster than the rise time of the spectrometer, and therefore, only a signal due to $P_{700}^{+}(Fe/S)^{-}$ that appears within the spectrometer rise time is observed from PS I complexes as a result of B branch electron transfer.

Figure 5 (top) shows the spin polarization pattern of PS I from the wild type and the $L722W_{PsaA}$ variant at 293 K. The spectra are taken at time windows centered at 100, 300, and 1240 ns after the laser flash. The solid curves are simulations,[35] and the dashed curves are experimentally observed spectra. In wild type PS I (Figure 5, top right), the spectrum at 100 ns is predominantly due to the radical pair $P_{700}^{+}A_{1A}^{-}$. With increasing time, the polarization pattern evolves into the mainly emissive spectrum due to $P_{700}^{+}(Fe/S)^{-}$.

The decay of the $P_{700}^{+}A_{1A}^{-}$ radical pair is seen most clearly by the disappearance of the emissive feature associated with A_{1A}^{-} at field position a. In the $L722W_{PsaA}$ variant (Figure 5, top left), the early radical pair spectrum representing $P_{700}^{+}A_{1A}^{-}$ has almost completely decayed within ~100 ns following the laser flash and is only visible as an extremely weak emissive feature at field position a. The major contribution to the spectra in all three time windows shown in Figure 5, top left arises from P_{700}^{+} in the $P_{700}^{+}(Fe/S)^{-}$ radical pair, indicating that the electron transfer from A_{1A}^{-} to F_X is much faster than in the wild-type. A comparison of the late spectrum at 1240 ns of PS I from the wild type and $L722W_{PsaA}$ variant indicates that its polarization pattern is unaltered, showing that the spin dynamics in the preceding radical pairs remain unaffected (see ref 36 for a review). The faster rate of electron transfer in the $L722W_{PsaA}$ variant is also apparent in the comparison of the transients shown in Figure 5, bottom. At position a, only $P_{700}^{+}A_1^{-}$ contributes to the signal, and it is evident that its lifetime is close to the rise time of the EPR spectrometer (50 ns), which results in a very weak response.

The lifetime of the A_{1A}^{-}-to-F_X electron transfer event in the two samples can be determined from a global simulation of the time/field data set as described in ref 35. In these simulations, only the rate of electron transfer from A_{1A}^{-} to F_X, the spin−lattice relaxation time, and the percentage of electron transfer in the two branches are allowed to vary, and their values are determined from a fit to the data set. The results of the simulation are shown as the solid spectra (Figure 5, top) and solid time traces (Figure 5, bottom). The lifetime of A_{1A}^{-}-to-F_X electron transfer obtained from the fit is τ = 270 ± 30 ns for the wild type and τ = 50 ± 30 ns for the $L722W_{PsaA}$ variant. Given the number of variables involved in the EPR simulations, these lifetimes are in reasonable agreement with those obtained from the time-resolved absorbance measurements. In the fits of the transient EPR data sets, the lifetime of the A_{1B}^{-}-to-F_X electron transfer was held constant at 20 ns, and values of less than 10% B-branch transfer gave best agreement with the experimental data for both the wild type and the $L722W_{PsaA}$ variant.

Temperature Dependence of the Rate of Electron Transfer from A_{1A}^{-} to F_X. In wild type PS I, the slow kinetic component due to the A_{1A}^{-}-to-F_X step is known to be strongly activated,[15,16] and a change in the activation energy is the most likely reason for the faster rate of electron transfer in the $L722W_{PsaA}$ variant. The faster rate implies a decrease in the activation energy, which would lead to weaker temperature dependence. In wild type PS I, the slow kinetic phase of electron transfer is directly observable in the spin-polarized transient EPR signals at temperatures above 220 K. Below this temperature, the rate of forward electron transfer becomes slower than the spin relaxation processes, and the signal falls below the detection limit

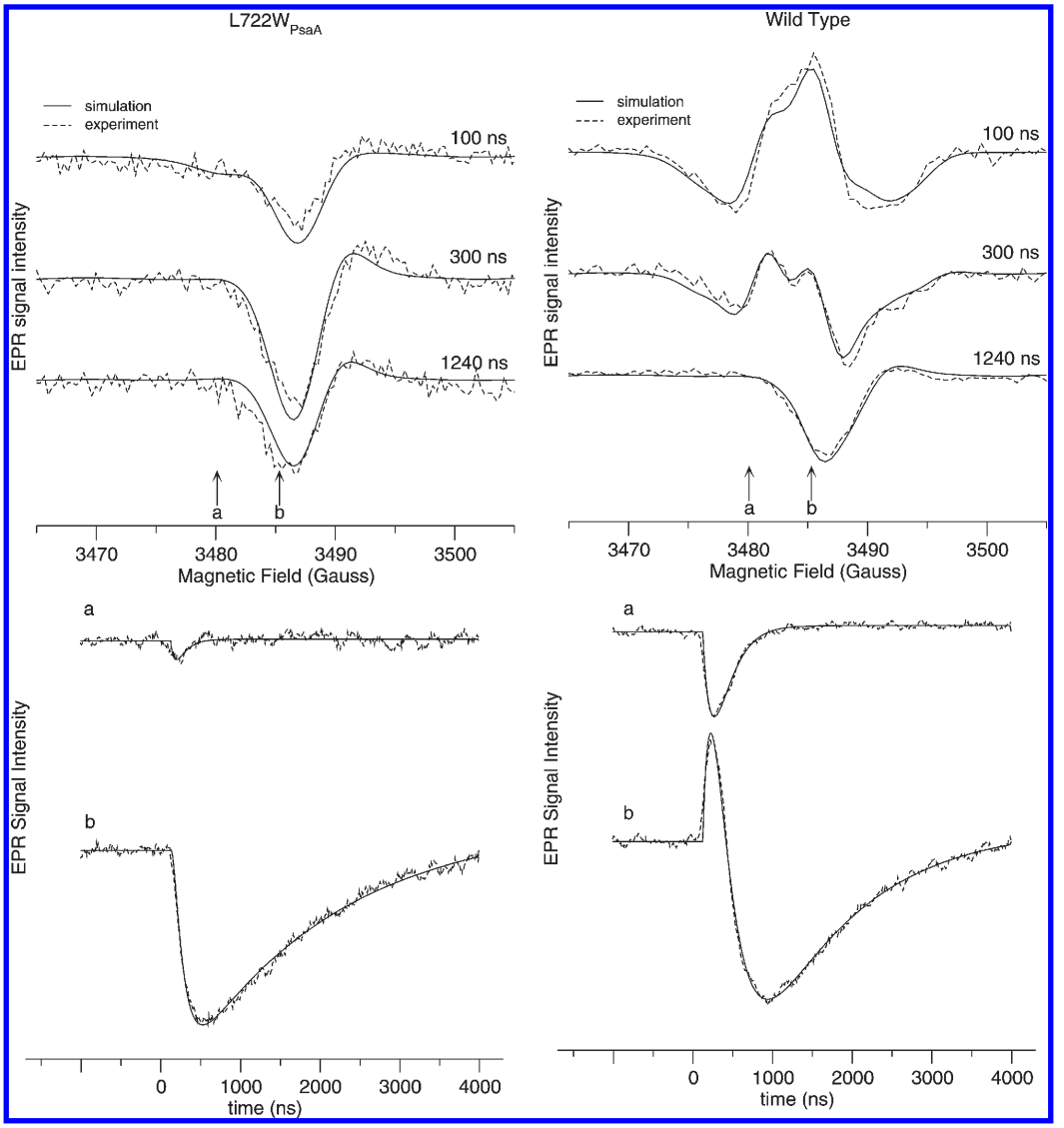

Figure 5. Top: Transient EPR spectrum of L722W$_{PsaA}$ (left) at X-band observed at 293 K compared with the wild type (right). Positive signals correspond to absorption (A), and negative signals correspond to emission (E). The E/A/E pattern is assigned to the $P_{700}^{+}A_1^{-}$ radical pair, and the (E/A) pattern is assigned to $P_{700}^{+}(Fe/S)^{-}$. Bottom: transients and fits of wild type (right) and L722W$_{PsaA}$ (left) used for determining the lifetime of the decay.

of the instrument. In contrast, the forward electron transfer kinetics from A_{1A}^{-} to F_X in the L722W$_{PsaA}$ variant is sufficiently fast that it can be clearly seen at temperatures down to 100 K.

Figure 6 shows the Arrhenius plot of the natural logarithm of the electron transfer rate versus the inverse temperature. For wild type PS I, data taken from ref 15 are plotted along with the rates from the optical and transient EPR measurements reported here. The lifetimes determined from the EPR data for the L722W$_{PsaA}$ variant are as follows: 100 K, 2.8 μs; 120 K, 2.0 μs; 140 K, 1.5 μs; 160 K, 0.7 μs; 180 K, 0.6 μs; 200 K, 0.8 μs; 220 K, 0.5 μs; 260 K, 170 ns; 293 K, 50 ns. The solid and dashed curves through these data are fits of the classical and semiclassical Marcus equation, respectively. The fit to the classical Marcus equation specifies an activation energy of 220 $\pm$ 10 meV for the wild type. For the L722W$_{PsaA}$ variant, the points do not lie on a single straight line, and the slope is considerably different above and below ~200 K. Above this temperature, the fit to the classical Marcus equation gives an activation energy of 180 $\pm$ 10 meV. Below ~200 K, the rate is almost independent of temperature. The fit to the semiclassical Marcus equation specifies an activation energy of 240 $\pm$ 10 meV and $\hbar\omega$ = 21 $\pm$ 1 meV for the wild type and an activation energy of 230 $\pm$ 10 meV and $\hbar\omega$ = 40 $\pm$ 1 meV for the L722W$_{PsaA}$ variant.

DISCUSSION

The nonadiabatic rate of electron transfer can be described by classical Marcus theory[37] according to eq 1.

$$k_{et} = \frac{2\pi|V|^2}{\hbar\sqrt{4\pi\lambda k_B T}} \exp\left\{-\left(\Delta G^0+\lambda\right)^2/4\lambda k_B T\right\} \qquad (1)$$

where V represents the electronic coupling between the initial and final state electronic wave functions. V is expected to decrease exponentially with the edge-to-edge distance, R, between the redox pairs, according to the relation $V = V^0\exp\{-\beta R\}$, where V^0 is the maximal value of the electronic coupling, depending on

dx.doi.org/10.1021/jp109531b |J. Phys. Chem. B 2011, 115, 1751–1759

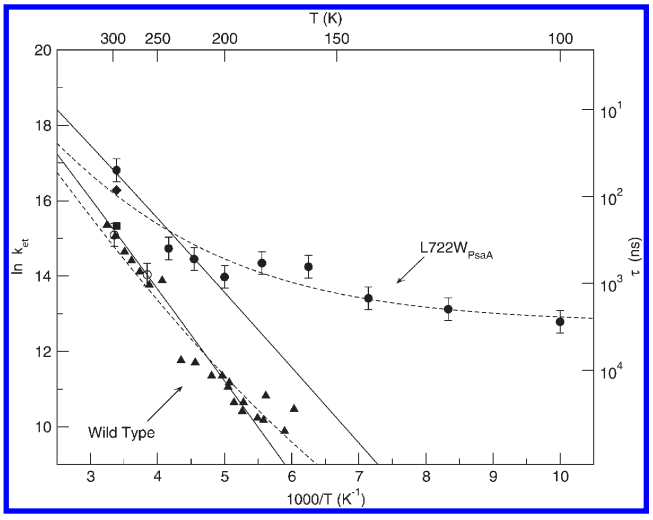

Figure 6. Arrhenius plot of the electron transfer rate from A_{1A}^- to F_X in the L722W$_{PsaA}$ variant and the wild type. Filled circles: L722W$_{PsaA}$ EPR data. Diamonds: L722W$_{PsaA}$ optical data. Open circles: wild type EPR data. Squares: wild type optical data (this work). Triangles: wild type data taken from ref 15. The solid lines through the data are fits of the classical Marcus equation (eq 1), and the dashed lines are fits of a quantum mechanical treatment. The electronic coupling and reorganization energy were fixed at 0.6 and 700 meV for all four fits.

the tunneling barrier. Extensive studies of photosynthetic electron transfer[38] indicate a common value of $\beta \approx 1.4$ Å^{-1} for a large number of reactions in different environments. The term $(\Delta G^0 + \lambda)^2/4\lambda$ in eq 1 represents the activation energy, E_a. λ and ΔG^0 are the reorganization energy and the Gibbs free energy change, respectively.[37] $2k_B\lambda T = \sigma^2(T)$ is the Gaussian width of the thermal nuclear fluctuations. λ is difficult to measure experimentally; however, a wide range of reactions in purple bacterial reaction centers have been shown to be consistent with a common value of ~0.7 eV.[38] For the A_{1A}^--to-F_X step in wild type PS I, the activation energy (~0.2 eV) is close to $\lambda/4$ (~0.18 eV), indicating that the reorganization energy dominates E_a.

The two properties that contribute to the rate of electron transfer between two cofactors and are most easily altered by a mutation are the intercofactor distance, which influences the electronic coupling, and ΔG^0, which influences E_a. There is no significant change in the orientation[17] or position (this study) of the phylloquinone in the A_{1A} binding pocket with respect to P_{700}. Because the Leu-to-Trp substitution is distant from the F_X cluster, significant structural changes in the F_X binding pocket are also not expected. Thus, the distance between A_{1A} and F_X in the L722W$_{PsaA}$ variant is probably not significantly altered compared with the wild type. Accordingly, no change in the electronic coupling is anticipated. The change in the electron transfer rate would instead be due to a change in E_a resulting from a change in the midpoint potential of the A_{1A} phylloquinone.

The fits of the classical Marcus equation (eq 1) to the Arrhenius plots (Figure 6, solid lines) are consistent with this expectation. The value of E_a in the L722W$_{PsaA}$ variant (180 ± 10 meV) is slightly smaller than in the wild type (220 ± 10 meV), whereas the electronic coupling (0.5 meV) is unchanged. The value of λ was kept fixed at 0.7 eV.[38] With this assumption, the values of E_a derived from Figure 6 yield $\Delta G^0 > 0$ with ΔG^0 for the wild type ~75 meV greater than that for the variant. If $\lambda = 1.0$ eV is assumed, the E_a values are unchanged and correspond to $\Delta G^0 < 0$ and ΔG^0 for the L722W$_{PsaA}$ variant ~90 meV more negative than that for the wild type. This suggests that the weakening of the H-bond caused by the mutation drives the midpoint potential of the phylloquinone more negative by ~75−90 mV, provided that it does not alter the reorganization energy. This estimate is in general agreement with a perturbation of the A_{1A}^- redox potential of 40−50 mV, derived from modeling the kinetics in the L722T$_{PsaA}$ (and L722Y$_{PsaA}$) variants of *C. reinhardtii*[19]

A striking feature of Figure 6 is the fact that in the L722W$_{PsaA}$ variant, the electron transfer rate becomes nearly independent of temperature below ~200 K, but it is strongly activated above this temperature. Similar behavior has been observed in other electron transfer reactions, such as the charge recombination between pheophytin and the special pair[39] and the oxidation of cytochrome[40] in purple bacteria. It has been suggested that the change in slope may be due to the fact that the vibrational energy is quantized, and therefore, at low temperature, it becomes constant at the ground state energy rather than approaching zero. When this effect is taken into account,[37,41,42] the Gaussian width in the Marcus equation becomes $\sigma^2(T) = \hbar\omega\lambda \coth(\hbar\omega/2k_BT)$, and the rate of electron transfer is described by eq 2.

$$k_{et} = \frac{2\pi|V|^2}{\hbar\sqrt{2\pi\sigma^2(T)}} \exp\left\{-(\Delta G^0+\lambda)^2/2\sigma^2(T)\right\} \qquad (2)$$

where ω is the angular frequency of the vibrational mode that couples to the electron transfer. The dashed lines in Figure 6 are fits of eq 2 to the data. In the fits, only the values of the classical activation energy, $(\Delta G^0 + \lambda)^2/4\lambda$, and the frequency of the mode were varied; the other parameters were kept fixed at the values used in the fits with eq 1. For the wild type, we calculate E_a = 240 ± 10 meV, and $\hbar\omega$ = 21 ± 1 meV (ω = 170 ± 10 cm^{-1}). It is worth noticing that for the wild type, $\hbar\omega = k_BT$ and that classical (eq 1) and semiclassical (eq 2) treatments yield the same results. For the L722W$_{PsaA}$ variant, the best agreement with the data is obtained with E_a = 230 ± 10 meV and $\hbar\omega$ = 40 ± 1 meV (ω = 340 ± 10 cm^{-1}). These values suggest that the electron transfer couples to higher frequency modes in the L722W$_{PsaA}$ variant than in the wild type. However, this result should be treated with caution.

First, in eq 2, it is assumed that the Gaussian width, $\sigma^2(T)$, associated with the initial and final state free energy surfaces are the same,[41,42] which implies no change in entropy. However, it has been shown from photoaccoustic spectroscopy data that the entropic contribution ($T\Delta S$) to the free energy change is dominant and therefore drives the A_{1A}^--to-F_X electron transfer step.[43] Moreover, the corresponding Arrhenius plot reported for anthraquinone-substituted PS I[44] is very similar to the data for the L722W$_{PsaA}$ variant shown in Figure 6, and the change in the slope, which determines ω, is found at roughly the same temperature as for several other unrelated electron transfer processes.[39,40] Therefore, it is prudent to consider alternative explanations.

It is known that a dynamical transition occurs in proteins[45−47] at ~200 K, and recent molecular dynamics simulations[48,49] suggest that the change in slope might be linked to this transition. Above the transition temperature, the motion of the protein is dominated by the slow anharmonic collective oscillations of groups of atoms, whereas below the transition, faster harmonic motions of individual atoms are dominant.[47] The molecular dynamic simulations[48,49] indicate that the slow motions lead to very broad energy surfaces for electron transfer reactions with lifetimes greater than the characteristic time of the slow protein

motions (~1 ns), which effectively lowers the activation barrier. A change in slope of the Arrhenius plot is predicted to occur at the transition temperature due to a significant drop in the solvent reorganization energy.[49] Thus, in this model, it is not the quantum mechanical nature of the vibrational modes but the dynamical transition in the protein that accounts for the change in slope.

It is also important to consider why the change in slope is observed so prominently in the L722W$_{PsaA}$ variant but is less pronounced or not visible in the A_{1A}^-- and A_{1B}^--to-F_X electron transfer steps in wild type PS I. Compared with the A_{1A}^--to-F_X electron transfer in the L722W$_{PsaA}$ variant, the A_{1B}^--to-F_X step in the wild type is faster and nearly independent of temperature,[16] whereas the A_{1A}^--to-F_X electron transfer in the wild type is slower, more strongly activated, and is blocked below ~200 K.[15] Thus, the behavior of the L722W$_{PsaA}$ kinetics is roughly between that of the wild type A- and B-branches.

A critical feature of the model in which slow protein fluctuations are invoked to explain the change in slope is the rate of the reaction compared with the characteristic frequency of the protein fluctuations. Fast reactions do not couple to the slow fluctuations, and the influence of the dynamic transition should become larger as the reaction becomes slower.[48,49] It appears that the lifetimes of A_1^--to-F_X electron transfer in the A- and B-branches in the wild type may span the critical region in which the dynamic transition becomes prominent. In this context, it should be noted that Schlodder et al.[15] showed that at different glycerol concentrations, the transition from forward electron transfer to charge recombination occurs in PS I at the glass transition temperature, in accordance with a phase transition in the medium. In this case, the change in slope in the L722W$_{PsaA}$ variant would not be specifically related to the H-bond, but rather, a result of the lower potential and faster electron transfer rate.

CONCLUSIONS

The H-bond plays a significant role in modulating the redox properties of the phylloquinones, affecting both the kinetics and energetics of electron transfer in PS I. The acceleration of forward electron transfer through phylloquinone can be rationalized in terms of classical Marcus theory with the shift in the midpoint potential of the phylloquinone in the L722W$_{PsaA}$ variant to a more negative value. The H-bond may play a role in determining the reorganization energy and frequency of the mode coupled to the electron transfer as evidenced from the temperature dependence of the forward electron transfer.

ASSOCIATED CONTENT

Supporting Information. Quantification of the triplet, OOP echo measurements of distance, and flash-induced absorption changes in whole cells in the nanosecond to microsecond are provided. This material is available free of charge via the Internet at http://pubs.acs.org.

AUTHOR INFORMATION

Corresponding Author

*(A.v.d.E.) Phone: 1 905 688 5550. Fax: 1 905 682 9020. E-mail: avde@brocku.ca. (J.H.G.) Phone: 1 814 865 1163. fax: 1 814 863 7024. E-mail: jhg5@psu.edu.

Present Addresses

[+]Instituto di Biofisica, Consiglio Nazionale delle Ricerche, Via Celoria 26, 20133 Milano, Italy.

ACKNOWLEDGMENT

This work was supported in part by a grant from the National Science Foundation (MCB-1021725) to J.H.G., a Discovery grant from NSERC to A.v.d.E., and by a grant from the Department of Energy, Energy Biosciences Division (DE-FG02-08ER-15989) to K.R. F.R. acknowledges financial support from the CNRS.

REFERENCES

(1) Golbeck, J. H. *Proc. Natl. Acad. Sci. U.S.A.* **1993**, *90*, 1642.
(2) Muller, M. G.; Niklas, J.; Lubitz, W.; Holzwarth, A. R. *Biophys. J.* **2003**, *85*, 3899.
(3) Redding, K.; van der Est, A. The directionality of electron transport in Photosystem I. In *Photosystem I: The Light-Induced Plastocyanin:Ferredoxin Oxidoreductase*; Golbeck, J., Ed.; Springer: Dordrecht, 2006; Vol. 24; p 413.
(4) Guergova-Kuras, M.; Boudreaux, B.; Joliot, A.; Joliot, P.; Redding, K. *Proc. Natl. Acad. Sci. U.S.A.* **2001**, *98*, 4437.
(5) Bautista, J. A.; Rappaport, F.; Guergova-Kuras, M.; Cohen, R. O.; Golbeck, J. H.; Wang, J. Y.; Beal, D.; Diner, B. A. *J. Biol. Chem.* **2005**, *280*, 20030.
(6) Li, Y.; van der Est, A.; Lucas, M. G.; Ramesh, V. M.; Gu, F.; Petrenko, A.; Lin, S.; Webber, A. N.; Rappaport, F.; Redding, K. *Proc. Natl. Acad. Sci. U.S.A.* **2006**, *103*, 2144.
(7) Srinivasan, N.; Golbeck, J. H. *Biochim. Biophys. Acta* **2009**, *1787*, 1057.
(8) Santabarbara, S.; Kuprov, I.; Fairclough, W. V.; Purton, S.; Hore, P. J.; Heathcote, P.; Evans, M. C. *Biochemistry* **2005**, *44*, 2119.
(9) Santabarbara, S.; Heathcote, P.; Evans, M. C. *Biochim. Biophys. Acta* **2005**, *1708*, 283.
(10) Setif, P.; Bottin, H. *Biochemistry* **1989**, *28*, 2689.
(11) Brettel, K. *Biochim. Biophys. Acta* **1997**, *1318*, 322.
(12) Brettel, K.; Leibl, W. *Biochim. Biophys. Acta* **2001**, *1507*, 100.
(13) Ptushenko, V. V.; Cherepanov, D. A.; Krishtalik, L. I.; Semenov, A. Y. *Photosynth. Res.* **2008**, *97*, 55.
(14) Ishikita, H.; Knapp, E. W. *J. Biol. Chem.* **2003**, *278*, 52002.
(15) Schlodder, E.; Falkenberg, K.; Gergeleit, M.; Brettel, K. *Biochemistry* **1998**, *37*, 9466.
(16) Agalarov, R.; Brettel, K. *Biochim. Biophys. Acta* **2003**, *1604*, 7.
(17) Srinivasan, N.; Karyagina, I.; Bittl, R.; van der Est, A.; Golbeck, J. H. *Biochemistry* **2009**, *48*, 3315.
(18) Shrinivasan, N.; Karyagina, I.; Golbeck, J.; Stehlik, D. Structure-function correlations in the $A_0 \rightarrow A_1 \rightarrow F_x$ electron transfer kinetics of the phylloquinone (A_1) acceptor in the cyanobacterial Photosystem I; In *Photosynthesis. Energy from the Sun: 14th International Congress on Photosynthesis*; Allen, J. F., Gantt, E., Golbeck, J. H., Osmond, B., Eds.; Springer: Dordrecht, 2007; pp 207−210.
(19) Santabarbara, S.; Reifschneider, K.; Jasaitis, A.; Gu, F.; Agostini, G.; Carbonera, D.; Rappaport, F.; Redding, K. E. *J. Phys. Chem. B* **2010**, *114*, 9300.
(20) Johnson, T. W.; Shen, G.; Zybailov, B.; Kolling, D.; Reategui, R.; Beauparlant, S.; Vassiliev, I. R.; Bryant, D. A.; Jones, A. D.; Golbeck, J. H.; Chitnis, P. R. *J. Biol. Chem.* **2000**, *275*, 8523.
(21) Bittl, R.; Zech, S. *J. Phys. Chem. B* **1997**, *101*, 1429.
(22) Agalarov, R.; Byrdin, M.; Rappaport, F.; Shen, G.; Bryant, D. A.; van der Est, A.; Golbeck, J. *Photochem. Photobiol.* **2008**, *84*, 1371.
(23) Béal, D.; Rappaport, F.; Joliot, P. *Rev. Sci. Instrum.* **1999**, *70*, 202.
(24) Grzybek, S.; Baymann, F.; Müller, K. H.; Mantele, W. A computer program for the analysis of redox titrations. In *Fifth International Conference on the Spectroscopy of Biological Molecules*;

Theophanides, T., Anastassopoulou, J., Fotopoulos, N., Eds.; Kluwer Academic Publishers: Dordrecht, 1993; pp 25−26.
(25) Carbonera, D.; Collareta, P.; Giacometti, G. *Biochim. Biophys. Acta* **1997**, *1322*, 115.
(26) Santabarbara, S.; Bordignon, E.; Jennings, R. C.; Carbonera, D. *Biochemistry* **2002**, *41*, 8184.
(27) Santabarbara, S.; Agostini, G.; Heathcote, P.; Carbonera, D. *Photosynth. Res.* **2005**, *86*, 283.
(28) Setif, P.; Bottin, H.; Mathis, P. *Biochim . Biophys . Acta* **1985**, *808*, 112.
(29) Brettel, K.; Setif, P. *Biochim . Biophys . Acta* **1987**, *893*, 109.
(30) Bittl, R.; Zech, S. G. *Biochim. Biophys. Acta* **2001**, *1507*, 194.
(31) Byrdin, M.; Jordan, P.; Krauss, N.; Fromme, P.; Stehlik, D.; Schlodder, E. *Biophys. J.* **2002**, *83*, 433.
(32) Byrdin, M.; Santabarbara, S.; Gu, F.; Fairclough, W. V.; Heathcote, P.; Redding, K.; Rappaport, F. *Biochim. Biophys. Acta* **2006**, *1757*, 1529.
(33) Bock, C.; van der Est, A; Brettel, K; Stehlik, D. *Febs Lett.* **1989**, *247*, 91.
(34) van der Est, A.; Bock, C.; Golbeck, J.; Brettel, K.; Setif, P.; Stehlik, D. *Biochemistry* **1994**, *33*, 11789.
(35) Van der Est, A.; Valieva, A. I.; Kandrashkin, Y. E.; Shen, G.; Bryant, D. A.; Golbeck, J. H. *Biochemistry* **2004**, *43*, 1264.
(36) Kandrashkin, Y. E.; van der Est, A. *Appl. Magn. Reson.* **2007**, *31*, 105.
(37) Marcus, R. A.; Sutin, N. *Biochim. Biophys. Acta* **1985**, *811*, 265.
(38) Moser, C. C.; Keske, J. M.; Warncke, K.; Farid, R. S.; Dutton, P. L. *Nature* **1992**, *355*, 796.
(39) Volk, M.; Aumeier, T.; Langenbacher, T.; Feick, R.; Ogrodnik, A.; Michel-Beyerle, M. E. *J. Phys. Chem. B* **1998**, *102*, 735.
(40) DeVault, D.; Chance, B. *Biophys. J.* **1966**, *6*, 825.
(41) Hopfield, J. J. *Proc. Natl. Acad. Sci. U.S.A.* **1974**, *71*, 3640.
(42) Parson, W. W.; Warshel, A. *J. Phys. Chem. B* **2004**, *108*, 10474.
(43) Hou, H. J.; Mauzerall, D. *J. Am. Chem. Soc.* **2006**, *128*, 1580.
(44) Pushkar, Y. N.; Karyagina, I.; Stehlik, D.; Brown, S.; van der Est, A. *J. Biol. Chem.* **2005**, *280*, 12382.
(45) Doster, W.; Cusack, S.; Petry, W. *Nature* **1989**, *337*, 754.
(46) Ferrand, M.; Dianoux, A. J.; Petry, W.; Zaccai, G. *Proc. Natl. Acad. Sci. U.S.A.* **1993**, *90*, 9668.
(47) Rasmussen, B. F.; Stock, A. M.; Ringe, D.; Petsko, G. A. *Nature* **1992**, *357*, 423.
(48) Lebard, D. N.; Matyushov, D. V. *Phys. Rev. E: Stat. Nonlin. Soft Matter Phys.* **2008**, *78*, 061901.
(49) Lebard, D. N.; Matyushov, D. V. *J. Phys. Chem. B* **2009**, *113*, 12424.